PROCEEDINGS OF SCIENCE

$B \to X_s\gamma$ and $B \to X_s\ell^+\ell^-$ at BABAR

Gerald Eigen[∗ †]
University of Bergen
E-mail: gerald.eigen@ift.uib.no
Representing the BABAR collaboration

We present new $B \to X_s\gamma$ measurements using both a fully inclusive approach and a sum of 38 exclusive final states. We update total and partial branching fractions, photon energy moments and the *CP* asymmetry. We extract the b quark mass and the kinetic energy of the b quark inside the B meson. For $B \to K^{(*)}\ell^+\ell^-$ decays, we present our final results on branching fractions, isospin asymmetries, *CP* violation asymmetry and lepton flavor ratios. For $B \to K^*\ell^+\ell^-$ modes, we have updated the angular analysis to determine the K^* longitudinal polarization and the lepton forward-backward asymmetry using the full BABAR data sample.

36th International Conference on High Energy Physics,
July 4-11, 2012
Melbourne, Australia

[∗]Speaker.

[†]This work was supported by Norwegian Research Council. I would like to thank G. Hiller and D. van Dyk for supplying the latest $B \to K^{(*)}\ell^+\ell^-$ theory predictions and L. Sun for his technical help.

PoS(ICHEP2012)329

1. Introduction

The decays $B \to X_S\gamma$ and $B \to K^{(*)}\ell^+\ell^-$, where $\ell^+\ell^-$ is e^+e^- or $\mu^+\mu^-$, are flavor-changing neutral-current processes that are forbidden in the Standard Model (SM) at tree level. They are described by an effective Hamiltonian that factorizes short-distance contributions from long-distance effects. The $B \to X_S\gamma$ decay proceeds via the electromagnetic penguin diagram in which the short-distance part is determined by the effective Wilson coefficient C_7^{eff}. In $B \to K^{(*)}\ell^+\ell^-$ modes, the Z penguin and the box diagram also contribute whose short-distance parts are parametrized in terms of the effective Wilson coefficients C_9^{eff} (vector part) and C_{10}^{eff} (axial-vector part). Physics beyond the SM introduces new loops and box diagrams with new particles (*e.g.* charged Higgs boson, supersymmetric particles) that may modify the effective Wilson coefficients. In addition, scalar and pseudo scalar diagrams may contribute introducing new Wilson coefficients C_S and C_P, respectively. To determine the Wilson coefficients precisely, we need to measure many observables in different modes. These rare decays probe New Physics at a scale of a few TeV.

2. $B \to X_s\gamma$

BABAR has updated the $B \to X_s\gamma$ measurements both in a fully inclusive and a semi-inclusive analysis using 383×10^6 $B\bar{B}$ events [1] and 471×10^6 $B\bar{B}$ events [2], respectively. In the SM at $\mathscr{O}(\alpha_s^2)$, the branching fraction is predicted to be $\mathscr{B}(B \to X_S\gamma) = (3.15 \pm 0.23) \times 10^{-4}$ for photon energies in the B-rest frame, $E_\gamma > 1.6$ GeV [3]. The measurement of $\mathscr{B}(B \to X_S\gamma)$ provides constraints on the charged Higgs mass $m_{H^\pm}$. The shape of the E_γ spectrum depends on the b quark mass m_b and its momentum inside the B meson. The shape function is expected to be similar to that for $B \to X_u\ell\nu$. Thus, precise measurements of the E_γ spectrum help us with extracting $|V_{ub}|$.

In the fully inclusive analysis, we update total and partial branching fractions, photon energy moments and the $B \to X_{s+d}\gamma$ *CP* asymmetry [1]. To suppress $e^+e^- \to q\bar{q}$ (u,d,s,c) continuum and $B\bar{B}$ backgrounds, we tag the recoiling B in semileptonic decays and use optimized π^0 and η vetoes, missing energy requirements and the output of two neural networks. For a signal efficiency of 2.5%, the efficiency for accepting continuum ($B\bar{B}$) background is reduced to 5×10^{-6} (1.3×10^{-4}). We estimate the residual continuum background by studying data taken 40 MeV below the $\Upsilon(4S)$ peak. Figure 1 (left) shows the $B \to X_s\gamma$ partial branching fraction after background subtraction and correcting for efficiency, resolution effects and Doppler smearing. For comparison, we show the predicted E_γ spectrum in the kinetic scheme using HFAG world averages for the shape function parameters [4]. For $E_\gamma > 1.8$ GeV, *BABAR* measures a total branching fraction of $\mathscr{B}(B \to X_S\gamma) = (3.21 \pm 0.15_{stat} \pm 0.29_{sys} \pm 0.08_{mod}) \times 10^{-4}$ where uncertainties are statistical, systematic and model, respectively. This is in good agreement with previous measurements [5, 6, 7]. After extrapolation to $E_\gamma > 1.6$ GeV, the branching fraction increases to $\mathscr{B}(B \to X_S\gamma) = (3.31 \pm 0.16_{stat} \pm 0.30_{sys} \pm 0.09_{mod}) \times 10^{-4}$, in good agreement with the SM prediction. We use this result to constrain new physics in the type II two-Higgs doublet model [8] excluding $m_{H^\pm} < 327$ GeV/c^2 at 95% confidence level (*CL*) independent of $\tan\beta$.

For $E_\gamma > 1.8$ GeV, *BABAR* measures energy moments of $\langle E_\gamma \rangle = (2.267 \pm 0.019_{stat} \pm 0.032_{sys} \pm 0.003_{mod})$ GeV and $\langle (E_\gamma - \langle E_\gamma \rangle)^2 \rangle = (0.0484 \pm 0.0053_{stat} \pm 0.0077_{sys} \pm 0.0005_{mod})$ GeV^2 that are consistent with previous results [5, 6, 7]. Tagging the B flavor by the lepton charge, we define the *CP*

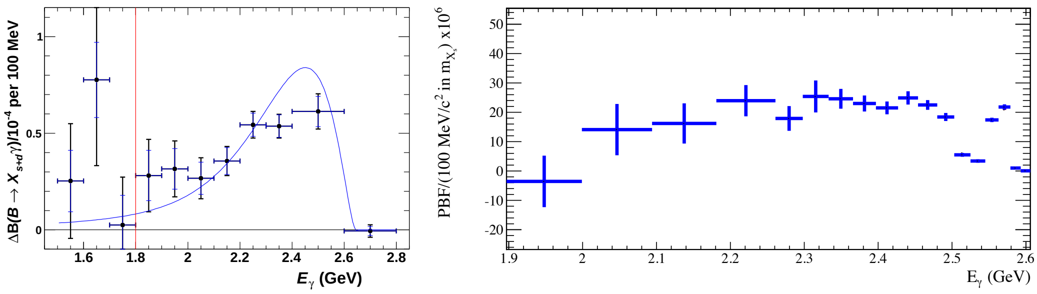

Figure 1: Partial branching fraction versus E_γ measured in a fully inclusive analysis (left) and for the sum of exclusive modes (right). Error bars (left) show statistical and total uncertainties. The solid curve shows a prediction for the kinetic scheme. The vertical bar separates signal from the control region.

Table 1: Determination of m_b and μ_π^2 in the kinetic-scheme [12] and shape function scheme [13] using the semi-inclusive analysis.

	BABAR kinetic scheme	*BABAR* shape function scheme	world average kinetic scheme	world average shape function scheme
m_b [GeV/c^2]	$4.568^{+0.038}_{-0.036}$	$4.579^{+0.032}_{-0.029}$	4.591 ± 0.031	$4.620^{+0.039}_{-0.032}$
μ_π^2 [GeV^2]	0.450 ± 0.054	$0.257^{+0.034}_{-0.039}$	0.454 ± 0.038	$0.288^{+0.054}_{-0.074}$

asymmetry $\mathscr{A}_{CP}(\bar{B} \to X_{s+d}\gamma) \equiv (\mathscr{N}(\bar{B} \to X_{s+d}\gamma) - \mathscr{N}(B \to X_{s+d}\gamma))/(\mathscr{N}(\bar{B} \to X_{s+d}\gamma) + \mathscr{N}(B \to X_{s+d}\gamma))$ in terms of event yields. After correcting for charge bias and mistagging, we obtain the most precise measurement of $\mathscr{A}_{CP}(\bar{B} \to X_{s+d}\gamma) = 0.057 \pm 0.06_{stat} \pm 0.018_{sys}$, which in agreement with previous results [9, 10] results and the SM prediction of zero [11].

In the semi-inclusive analysis, we combine 38 exclusive $B \to X_s\gamma$ final states [2]. We reconstruct the hadronic mass m_{X_s} in 100 MeV/c^2 bins and calculate the photon energy by $E_\gamma = \frac{m_B^2 - m_{X_s}^2}{2m_B}$. Figure 1 (right) shows the partial branching fraction versus E_γ. Table 1 summarizes the fit results of m_b and the kinetic energy of the b quark, μ_π^2, extracted from fits to the kinetic scheme [12] and shape function scheme [13]. We measure energy moments of $\langle E_\gamma \rangle = (2.346 \pm 0.018^{+0.027}_{-0.022})$ GeV and $\langle (E_\gamma - \langle E_\gamma \rangle)^2 \rangle = (0.0211 \pm 0.0057^{+0.0055}_{-0.0069})$ GeV^2 for $E_\gamma > 1.9$ GeV. Summing the partial branching fraction over all m_{X_S} bins yields $\mathscr{B}(\bar{B} \to X_s\gamma) = (3.29 \pm 0.19_{stat} \pm 0.48_{sys}) \times 10^{-4}$ for $E_\gamma > 1.9$ GeV, which is in good agreement with the results of the inclusive analysis.

3. $B \to K^{(*)}\ell^+\ell^-$ Rates and Rate asymmetries

Using the full *BABAR* data sample (471×10^6 $B\bar{B}$ events), we reconstructs eight $B \to K^{(*)}\ell^+\ell^-$ final states with $K^\pm, K_S^0, K^\pm\pi^\mp, K_S^0\pi^\pm$ recoiling against e^+e^- or $\mu^+\mu^-$ [14]. We suppress combinatorial $B\bar{B}$ and $q\bar{q}$ backgrounds with two boosted decision trees and veto the J/ψ and $\psi(2S)$ mass regions. For $B \to K^{(*)}\ell^+\ell^-$ modes, we perform one- (two-) dimensional fits of the beam energy-constrained mass (and $K\pi$ mass) to select signal yields. We use the vetoed J/ψ and $\psi(2S)$ samples and generated pseudo experiments to check the performance of our selection.

We measure partial branching fractions $d\mathscr{B}(B \to K^{(*)}\ell^+\ell^-)/ds$ in six $s = m^2_{\ell^+\ell^-}$ bins. Figure 2 shows our results in comparison to the average over all $d\mathscr{B}(B \to K^{(*)}\ell^+\ell^-)/ds$ measurements from *BABAR* [14], Belle [15], CDF [16], and LHCb [17] and to the SM prediction[18, 19]. Table 2

Table 2: *BABAR* results for $B \to K^{(*)}\ell^+\ell^-$ modes on total branching fractions, *CP* asymmetries, lepton flavor ratios, isospin asymmetries, the lepton forward-backward asymmetry and K^* longitudinal polarization. The first uncertainty is statistical, the second is systematic.

Mode s $[\frac{\mathrm{GeV}^2}{\mathrm{c}^4}]$	$\mathscr{B}[10^{-7}]$ all s	$\mathscr{A}_{CP}$ all s	$\mathscr{R}_{K^{(*)}}$ $s > 0.1$ GeV^2/c^4	$\mathscr{A}_I$ $0.1 \le s \le 8.12$	$\mathscr{A}_{FB}$ $1.0 \le s \le 6.0$	$\mathscr{F}_L$ $1.0 \le s \le 6.0$
$K\ell^+\ell^-$	$4.7^{+0.6+0.2}_{-0.6-0.2}$	$-0.03^{+0.14+0.01}_{-0.14-0.01}$	$1.00^{+0.31+0.07}_{-0.25-0.07}$	$-0.58^{+0.29+0.02}_{-0.37-0.02}$	-	-
$K^*\ell^+\ell^-$	$10.2^{+1.4+0.05}_{-1.3-0.05}$	$0.03^{+0.13+0.01}_{-0.13-0.01}$	$1.13^{+0.34+0.10}_{-0.26-0.10}$	$-0.25^{+0.17+0.03}_{-0.20-0.03}$	$0.26^{+0.27+0.07}_{-0.30-0.07}$	$0.25^{+0.09+0.03}_{-0.08-0.03}$

summarizes our total branching fraction and rate asymmetry measurements. We tag the flavor of each B meson to determine the *CP* asymmetry

$$\mathscr{A}_{CP} = \frac{\mathscr{B}(\bar{B} \to \bar{K}^{(*)}\ell^+\ell^-) - \mathscr{B}(B \to K^{(*)}\ell^+\ell^-)}{\mathscr{B}(\bar{B} \to \bar{K}^{(*)}\ell^+\ell^-) + \mathscr{B}(B \to K^{(*)}\ell^+\ell^-)} \tag{3.1}$$

that is expected to be very small in the SM [20, 21]. We extract the lepton flavor ratios

$$\mathscr{R}_{K^{(*)}} = \mathscr{B}(B \to K^{(*)}\mu^+\mu^-)/\mathscr{B}(B \to K^{(*)}e^+e^-) \tag{3.2}$$

with the constraint $s > 0.1$ GeV^2/c^4 yielding the SM prediction $R_{K^{(*)}} = 1$ [22]. Accounting for the different B lifetimes $r_\tau = \frac{\tau_{B^0}}{\tau_B^{\pm}}$, we define the isospin asymmetry

$$d\mathscr{A}_I/ds = \frac{d\mathscr{B}(B^0 \to \bar{K}^{(*)0}\ell^+\ell^-)/ds - r_\tau d\mathscr{B}(B^\pm \to K^{(*)\pm}\ell^+\ell^-)/ds}{d\mathscr{B}(\bar{B}^0 \to \bar{K}^{(*)0}\ell^+\ell^-)/ds + r_\tau d\mathscr{B}(B^\pm \to K^{(*)\pm}\ell^+\ell^-)/ds}. \tag{3.3}$$

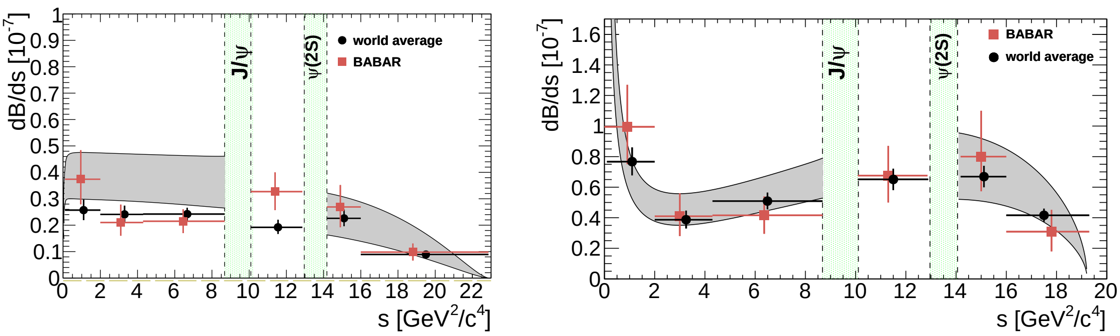

Figure 2: $d\mathscr{B}/ds$ for $B \to K\ell^+\ell^-$ (left) and $B \to K^*\ell^+\ell^-$ (right) for *BABAR* data (squares), the experimental average (points) and the SM prediction (grey curves). Vertical bands show the J/ψ and $\psi(2S)$ vetoes.

Figure 3 shows the isospin asymmetry for $B \to K^{(*)}\ell^+\ell^-$ modes in six s bins in comparison to the average over all experiments [14, 15, 16, 17]. In the SM, $\mathscr{A}_I$ is expected to be of the order of $\mathscr{O}(1\%)$ [23]. The $\mathscr{A}_I$ measurements below the J/ψ are listed in Table 2. For $B \to K\ell^+\ell^-$, consistency with the SM is at the 2.1σ level. All other measurements of branching fractions, *CP* asymmetries and lepton flavor ratios are in good agreement with the SM prediction [**?**, **?**, 18, 19].

4. $B \to K^{(*)}\ell^+\ell^-$ Angular Analyses

The $B \to K^*\ell^+\ell^-$ decay is characterized by three angles: θ_K the angle between the K and B in the K^* rest frame, θ_ℓ the angle between the ℓ^+ and the B in the $\ell^+\ell^-$ rest frame and ϕ the angle

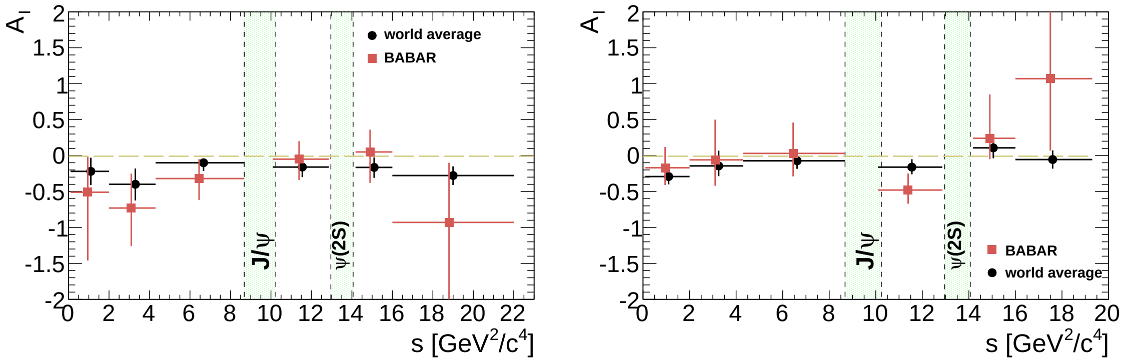

Figure 3: Isospin asymmetry for $B \to K\ell^+\ell^-$ (left) and $B \to K^*\ell^+\ell^-$ (right) for *BABAR* data (squares) and the experimental average (points). Vertical bands show the J/ψ and $\psi(2S)$ vetoes.

between the K^* and $\ell^+\ell^-$ decay planes. The one-dimensional $\cos\theta_K$ and $\cos\theta_\ell$ distributions depend on the K^* longitudinal polarization $\mathscr{F}_L$ and the lepton forward-backward asymmetry $\mathscr{A}_{FB}$ [22, 24]

$$\begin{aligned} W(\cos\theta_K) &= \frac{3}{2}\mathscr{F}_L\cos^2\theta_K + \frac{3}{4}(1-\mathscr{F}_L)\sin^2\theta_K, \\ W(\cos\theta_\ell) &= \frac{3}{4}\mathscr{F}_L\sin^2\theta_\ell + \frac{3}{8}(1-\mathscr{F}_L)(1+\cos^2\theta_\ell) + \mathscr{A}_{FB}\cos\theta_\ell. \end{aligned} \tag{4.1}$$

Using the full *BABAR* data sample, we reconstructs six $B \to K^*\ell^+\ell^-$ final states with $K^* \to K^\pm\pi^\mp, K^0_S\pi^\pm, K^\pm\pi^0$. The event selection is similar to that for rate asymmetries. We extract $\mathscr{F}_L$ and $\mathscr{A}_{FB}$ by performing a profile likelihood scan. Figure 4 shows our $\mathscr{F}_L$ and $\mathscr{A}_{FB}$ measurements in six s bins in comparison to the average over all experiments, the SM predictions with uncertainties and predictions for a model in which the sign of Wilson coefficient C_7^{eff} is flipped with respect to the expected SM value [22, 20]. All results are consistent with the SM prediction. In the low s region ($1 < s < 6$ GeV^2/c^4), the *BABAR* results are listed in Table 2. They are consistent with the SM predictions of $\mathscr{F}_L^{SM} = 0.73^{+0.13}_{-0.23}$ and $\mathscr{A}_{FB}^{SM} = -0.05^{+0.03}_{-0.04}$ [18, 20, 22, 25] and with the world averages of $\mathscr{F}_L^{WA} = 0.41 \pm 0.06$ and $\mathscr{A}_{FB}^{WA} = 0.11^{+0.08}_{-0.09}$ [4].

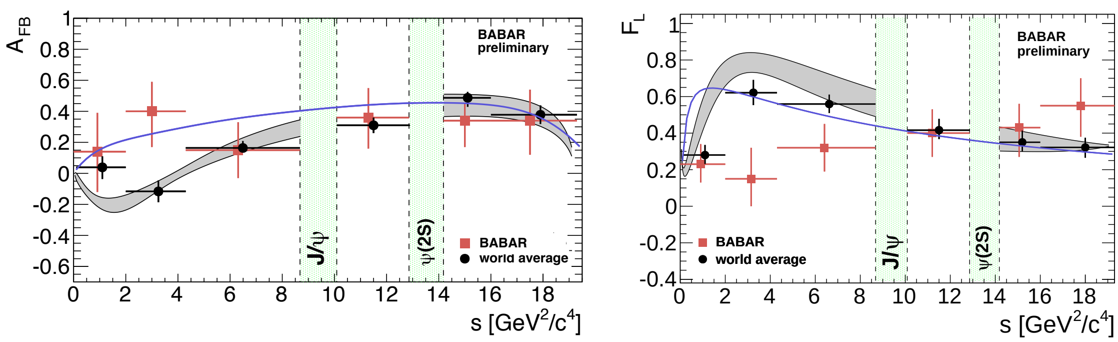

Figure 4: *BABAR* preliminary results (squares) for $\mathscr{A}_{FB}$ (left) and $\mathscr{F}_L$ (right) for $B \to K^*\ell^+\ell^-$ modes compared to the average over all experiments (points), the SM prediction (shaded curves) and a model for which the sign of C_7^{eff} is flipped (blue curve). Vertical bands show the J/ψ and $\psi(2S)$ vetoes.

5. Conclusion

The *BABAR* $B \to X_s\gamma$ results on branching fractions, photon energy moments, m_b, μ_π^2 and the *CP* asymmetry are in good agreement with the SM predictions. The charged Higgs mass is constrained to $M_{H^\pm} > 327$ GeV^2/c^2 at 95% *CL* independent of $\tan\beta$. For $B \to K^{(*)}\ell^+\ell^-$, the *BABAR* results on partial branching fraction, isospin asymmetries, lepton flavor ratios, *CP* asymmetries, K^* longitudinal polarization, and lepton forward-backward asymmetry are consistent with the SM predictions. Significant improvement on these measurements will come from LHCb and the Super *B*-factories. The large data samples will permit to study several new angular observables that provide higher discrimination power between the SM and new physics effects.

References

[1] J.P Lees *et al.*, Phys. Rev. Lett. **109**, 191801 (2012); arXiv:1207.5772 [hep-ex] (2012).

[2] J.P Lees *et al.*, Phys.Rev. D **86** (2012) 052012 (2012).

[3] M. Misiak *et al.*, Phys. Rev. Lett. **98**, 022002 (2007).

[4] D. Asner *et al.*, arXiv:1010.1589v3 (2011); www.slac.stanford.edu/xorg/hfag/triangle/index.html

[5] B. Aubert *et al.*, Phys. Rev. D **72**, 052004 (2005).

[6] A. Limosani *et al.*, Phys. Rev. Lett. **103**, 241801 (2009).

[7] S. Chen *et al.*, Phys. Rev. Lett. **87**, 251807 (2001).

[8] M. Misiak *et al.*, Phys. Rev. Lett. **98**, 022002 (2007); U. Haisch, arXiv:0805.2141v2 (2008).

[9] B. Aubert *et al.*, Phys. Rev. Lett. **97**, 171803 (2006); Phys. Rev. D **77**, 051103 (2008).

[10] T. E. Coan *et al.*, Phys.Rev. Lett. **86**, 5661 (2001).

[11] A.L. Kagan and M. Neubert, Phys. Rev. D **58**, 094012 (1998).

[12] D. Benson, I. Bigi and N. Uraltsev, Nucl. Phys. B **710**, 726 371 (2005).

[13] B. Lange, M. Neubert and G. Paz, Phys. Rev. D **72**, 073006 (2005).

[14] J. P. Lees *et al.*, Phys. Rev. D **86**, 052012 (2012).

[15] J. T. Wei *et al.*, Phys. Rev. Lett. **103**, 171801 (2009).

[16] T. Aaltonen *et al.*, Phys. Rev. Lett. **108**, 081807 (2012); Phys. Rev. Lett. 107, 201802 (2011).

[17] R. Aij *et al.*, JHEP 1207, 133 (2012).

[18] C. Bobeth, *et al.*, JHEP **1007**, 098 (2010); ibid, JHEP **1107**, 67 (2011).

[19] C. Bobeth, *et al.*, JHEP **1201**, 107 (2012).

[20] F. Krüger *et al.*, Phys. Rev. D **61**, 114028 (2000); Erratum-ibid. D **63**, 019901 (2001).

[21] C. Bobeth *et al.*, JHEP **807**, 106 (2008).

[22] A. Ali *et al.*, Phys. Rev. D **61**, 074024 (2000); A. Ali *et al.*, Phys. Rev. D **66**, 034002 (2002).

[23] Th. Feldmann and J. Matias, JHEP **301**, 074 (2003).

[24] C. Bobeth *et al.*, JHEP **0712**, 040 (2007).

[25] F. Krüger and J. Matias, Phys. Rev. D **71**, 094009 (2005); G. Buchalla *et al.*, Phys. Rev. D **63**, 014015 (2000).